

**Hydrogen Susceptibility of Nanostructured Bainitic**  
**Steels**

Mathew Peet<sup>1\*</sup> and Tomohiko Hojo<sup>2</sup>

<sup>1</sup>Department of Materials Science and Metallurgy, University of  
Cambridge, 27 Charles Babbage Road, Cambridge, United  
Kingdom, CB3 0FS.

<sup>1</sup>[mjp54@cam.ac.uk](mailto:mjp54@cam.ac.uk) (\*corresponding author)

<sup>2</sup>Department of Mechanical Engineering, Iwate University, Iwate,  
Japan.

<sup>2</sup>[th369@iwate-u.ac.jp](mailto:th369@iwate-u.ac.jp)

## **Abstract**

Nanostructured steels with an ultimate tensile strength of 1.6 GPa were produced with austenite content varying from 0-35 vol%. The effect on the mechanical properties were assessed after saturating the steel with hydrogen.

Elongation was reduced to 2-5% and UTS to 65-70% of prior value. Thermal desorption measurements confirmed the higher solubility of hydrogen in the steel with higher austenite content. The level of hydrogen saturation was found to correlate to the total area of grain boundaries rather than to the volume fraction of retained austenite.

**Keywords:** TRIP-aided steel, ultra high strength steel, retained austenite, hydrogen, bainite.

# 1 Introduction

Deleterious hydrogen is introduced into the microstructure of steel as a result of manufacture, welding, corrosion, or galvanic protection [1-3]. High strength steels are thought to be particularly susceptible [4-7].

Nanostructured bainitic steels possess high strength imparted by the fine bainite plates in a matrix of retained austenite [8-13]. Isothermal transformation is the only viable method of producing such a nanostructure in bulk [10, 14, 15]. These novel nanostructures result from transformation around 473-523 K (200–250°C), with a colossal supersaturation of carbon in the austenite, and high supersaturation of carbon in ferrite [16-20].

The large fractions of austenite possible in these steels allows improvement in mechanical properties by transformation induced plasticity [21], and the presence of austenite is known to result in increased trapping of hydrogen [7, 22]. The diffusion of hydrogen at 300 K is also much slower ( $2 \times 10^8$  times) in austenite than in ferrite [1, 23]. The percolating austenite structure has been observed to slow diffusion [24], and the effective diffusivity of ferrite is also reduced by the large number of defects present [24].

In the current work nanostructured steels with an ultimate tensile strength of 1.6 GPa were produced with austenite content varying from 0–35 vol%. Electrolytic hydrogen charging to saturation was applied to characterize the maximum detriment to the mechanical properties. Thermal desorption measurements were applied to characterize the potency of austenite as a trapping site in these steels.

## 2 Experimental Method

Tensile specimens were produced with 1.1 mm thickness, 6 mm width and 20 mm length of the parallel section by electro-discharge machining from cast and rolled ingots of two compositions, Steel A with composition Fe-0.83C-1.98Mn-1.02Cr-1.57Si-1.54Co-0.24Mo wt% and steel B having composition Fe-0.78C-2.02Mn-1.01Cr-1.60Si-3.87Co-1.37Al-0.24Mo wt%. The materials being from the same stock as previously developed and characterized by Garcia-Mateo *et al.* [9, 10]. The tensile specimens were austenitised for 30 min at 1223 K (950°C) in an argon tube furnace before transfer to fan-assisted oven at 563 K (290°C) and held for six hours. A number of samples of steel A were tempered at 773 K (500°C) to provide comparison against a microstructure with a negligible amount of retained austenite. Previous experiments reveal the high resistance to tempering of the bainitic microstructure in these steels [25], and tempering at 573 K (300°C) in this work was not sufficient to reduce the fraction of retained austenite.

Lattice parameters and volume fraction of austenite after isothermal transformation were determined by X-ray diffraction using a Phillips PW1830 diffractometer operated at 40 kV and 40 mA, with 10 mm mask,  $1/2^\circ$  divergence and anti-scatter slits and 0.2 mm receiving slit. Peak positions and intensities were determined using Phillips ProFit software, to derive lattice parameters and volume fractions for ferrite and austenite [26]. Lattice parameter were related to carbon content using linear equations following previous workers [27].

Hardness measurements were made using Vickers hardness machine using a load of 50 kg, with three indentations made, and the error estimated from the standard deviation of the six measurements.

The hydrogen susceptibility of the steels in each condition was assessed by comparing the tensile properties before and after hydrogen charging. Hydrogen charging was achieved by spot welding samples at one end to a stainless strip with all except the gauge length painted with lacquer to prevent contact with the electrolyte. The stainless steel strip was used to suspend the tensile samples in solution of 2.5 L distilled water, 78 g of sodium chloride and 7.8 g of ammonium thiocyanate. A voltage was applied using a constant current supply of 20 mA for 48 h to produce a current density of  $10 \text{ A/m}^2$ . The gauge length of the tensile samples formed the cathode, and a platinum wire was used as the anode.

Tensile testing was undertaken with an Instron 8501 hydraulic testing machine, with 2620-604 axial clip-on dynamic strain gauge extensometer using 15 mm gauge length at a crosshead speed of  $1 \text{ mm min}^{-1}$ , resulting in strain rate in the gauge length of  $0.022 \text{ min}^{-1}$ . The series of tests were started 10 min after charging, with the final test being complete approximately 1 h after charging was complete.

For analysis of the hydrogen content charging was repeated with the same conditions on spare tensile samples of the same dimensions which had been heat treated along with the mechanically tested samples. Total hydrogen content was determined by heating a small amount of material until melting. Hydrogen evolution as a function of temperature was measured using atmospheric pressure ionization mass spectrometry (APIMS) electronic gas analyzer during heating at  $0.2 \text{ K s}^{-1}$ .

Fractography was undertaken using a JEOL JSM-6510LA electron microscope.

### 3 Results

X-ray diffraction results, table 1, show that large volume fractions of austenite have been retained as a result of transformation at 563 K (290°C), with 35% austenite in alloy A and 30% in alloy B.

Tempering at 773 K (500°C) was applied to allow comparison against material with a low amount of retained austenite. Characterization of similarly tempered material gives confidence that the structure is likely ferrite and cementite although transition carbides are also possible [26]. The tempering condition was selected to remove austenite while achieving a comparable hardness, and tensile properties as far as possible, to those of the as-transformed condition (as shown in table 2). Tempering alloy A at 773 K (500°C) decreased the hardness by about 5%, reduced the elongation from around 20–25% to 4–5%, while the ultimate tensile strength was slightly decreased (also  $\approx 5\%$ ) but the yield strength increased by 25%. Figure 1 compares the stress–strain curves before and after hydrogen charging, and table 2 summarises the mechanical property results, in all cases elongation was greatly reduced by saturation with hydrogen.

In previous literature the concept of a ‘hydrogen embrittlement susceptibility factor’ (*HES*) has been introduced as the percentage of each property lost after exposure to hydrogen [28]. Table 2 compares *HES* as calculated from the change of yield strength, ultimate tensile strength or elongation. Steel A in the tempered condition had the lowest susceptibility as measured by elongation *HES* factor, but this is due to the low initial value of elongation. A negative value of the embrittlement factor was calculated when considering the change in the area reduction, indicating a slight expansion, however the initial and final values are of similar magnitude, and this is likely to be an artifact due to

measurement errors. Steel B in the as-transformed condition retained a larger proportion of the ultimate tensile strength than steel A.

Figures 2–4 show the typical appearance of the fracture surfaces of the tensile samples, for evaluation of fracture mechanism. Steel A and B in as-transformed condition showed ductility in the tensile results, and necking was observed in the tensile samples. This is consistent with the micro-void coalescence seen on the fracture surfaces of the un-tempered material. Ductility is lower in the tempered material, and fracture surface has a larger proportion of flat areas indicating a greater role of crack propagation during failure (i.e. brittle fracture).

There is a striking similarity of the fracture surfaces on the microscopic scale when comparing the as heat-treated and the hydrogen charged material in each case, except that the introduction of hydrogen has superimposed a large amount of secondary cracking. Fracture surfaces typically incorporate features both of ductile failure and of quasi-cleavage. Secondary cracking in hydrogen charged samples exhibit a faceted appearance and can be seen to propagate in both an intergranular mode along prior-austenite grain or packet boundaries and, most often, in an transgranular/intragranular mode, passing through similarly oriented regions on the scale of the bainite packets. This is common in carbide free bainitic steels due to the packets of bainite containing plates of similar orientation, which will lead to a larger 'crystallographic grain size' and decrease the ability of the structure to resist crack propagation [29, 30].

Comparing fracture surfaces for alloy A, in as-transformed condition the fracture surface shows evidence of microvoid coalescence, figure 2(a). This sample exhibited 20% of uniform elongation and slight necking before failure. After hydrogen charging, the fracture surface, figure 2(b), is more typical of that expected from brittle cleavage

failure, and could be characterized as quasi-cleavage with failure both through bainite packets and at the packet boundaries. Despite the elongation being only 0.4% in this condition there does still seem to be evidence of some areas of microvoid coalescence on the fracture surface.

In the tempered condition (AT, figure 3) there is very little difference in the appearance in the two conditions except the superposition of cracking in the hydrogen charged material. In both cases the fracture surfaces are best classified as quasi-cleavage.

In alloy B both fracture surfaces (figure 4) show evidence of both ductile failure by microvoid coalescence and some faceted appearance typical of quasi-cleavage. This material exhibited clear evidence of necking before failure in as-transformed material.

Comparison of figure 4 (a) and (b) shows remarkable similarity in the nature of the fracture surface in alloy B in as-transformed condition, considering the scale of microvoids. In alloy A, also transformed at 563 K (290°C) after hydrogen charging the surface has a more faceted appearance than without hydrogen. The length scale of the facets is similar to that of the bainite packets (rather than the prior austenite grain size or the plate size). Accompanying the faceted area there are many regions which have a more ductile appearance.

As can be noted from the fractographs, the position of cracking on the fracture surface was different in each of the materials tested, from the surface in as-transformed alloy A, along center line of fracture surface in tempered alloy A, and with more complicated cracking along center but with radial cracks towards corners in alloy B fracture surface. It is not known how reproducible the position of cracking would be if

the experiments were repeated several times, or if the position of these secondary cracks has any influence on mechanical properties.

Although on a microscopic scale ductility is indicated by the fracture surface of the hydrogen charged samples, the samples had very little elongation before failure. Macroscopically the fracture surface of alloy A and B in charged condition are very different, figure 5. Alloy B has complex fracture surface with flat areas indicating cleavage at edges of the sample and the more ductile area shown in previous figures occurring at the center. In contrast Alloy A had similar appearance on the whole of the fracture surface apart from the appearance of cracking in certain locations. Failure occurred at stress levels above 1 GPa, so large amounts of energy are released during tensile failure and it is therefore possible that the secondary cracking observed could occur as part of the fracture process and not necessarily as part of fracture initiation.

Regarding the level of hydrogen absorption, alloy A and B containing retained austenite absorbed more hydrogen than alloy A in tempered condition (AT) which had no retained austenite.

The peak of the hydrogen evolution curve of alloy A and B are shifted to higher temperature compared with that of the tempered material. The presence of retained austenite is clearly associated with the capacity to store hydrogen as there is a large effect on the total amount of absorption. The larger amount of hydrogen could be stored in the austenite or at austenite–ferrite boundaries. Since each evolution curve took the form of a single peak (or indistinguishable overlapping peaks), amounts of diffusible hydrogen were defined as hydrogen evolved at temperatures below 473 K (200°C). Distinguishing diffusible hydrogen in this way should be considered quite arbitrary, but it is not possible to distinguish from the curves observed if there is a single distribution

of trapping sites or several types of sites. As shown in table 3 and figure 6 the ratio of diffusible to total hydrogen is almost constant.

In the present study it is not strictly possible to relate the evolution curve to changes occurring in the microstructure during heating without further characterization of the samples. However from previous work examining the resistance to tempering, it seems most likely that the evolution of hydrogen during heating was not dependent on changes in the microstructure but dominated by the effect of the strength of trapping sites. As observed by X-ray diffraction, in this steel austenite is retained at a similar volume fraction even after heating to 573 K (300°C) and holding for five hours (table 1). So evolution of hydrogen seen in figure 7 is unlikely to be related to changes in phase fractions of austenite below this temperature.

The samples with retained austenite both had higher amounts of diffusible and non-diffusible hydrogen than the tempered sample, the simple correlation shows increase storage depending on the amount of austenite. However, alloy B with a slightly lower amount of retained austenite has a greater storage capacity than alloy A. The most likely explanation is that the hydrogen storage is associated with the larger area of interfaces introduced into the steel during transformation. Although the ferrite plate size is expected to be broadly similar as a result of transformation at the same temperature, previous results comparing alloy A with an alloy of composition Fe-0.78C-1.49Si-1.95Mn-0.97Cr-0.24Mo-0.99Al-1.60Co-0.02P-0.02S wt% transformed at 573 K (300°C) demonstrated that alloying with 1.6Co-1Al caused the bainite plate size to reduce from 57 nm to 53 nm [10]. Alloy B in this paper has a higher level of 3.87Co-1.37Al wt%, this can be expected to cause further reduction in the plate thickness due to additional strengthening of the austenite present during transformation [31]. Given the similarity in

the transformation temperature to that previously extensively characterized, it is reasonable to assume a 10% reduction in plate width between alloy A and B transformed at 563 K (290°C) and thereby calculate approximately the relative difference in surface area per unit volume ( $S_v$ ) between the different alloys and heat treatments. The amount of boundary surface area per unit volume of steel is proportional to the bainitic ferrite plate size and the volume fraction of ferrite  $V_\alpha$  (table 1).

$$\frac{S_{VA}}{S_{VB}} = \frac{(1/t_A)V_{\alpha A}}{(1/t_B)V_{\alpha B}} = \frac{(1/t_A) \times 0.649}{(1/0.9t_A) \times 0.7} = 0.834 \quad (1)$$

$$\frac{H_A}{H_B} = \frac{7.1}{8.5} = 0.835 \quad (2)$$

where  $S_{VA}$  and  $S_{VB}$  are the surface area per unit volume of grain boundaries in sample A and B.  $H_A$  and  $H_B$  are the total hydrogen contents,  $t_A$  and  $t_B$  are the thickness of the bainite plates, and  $V_{\alpha A}$  and  $V_{\alpha B}$  the volume fractions of ferrite in samples A and B.

This also explains the lower storage capacity of the tempered material, since the removal of austenite from between the plates will approximately halve the area of grain boundaries per unit volume, while the storage capacity reduced to 0.42 of that in the as-transformed state. The tempering treatment applied is sufficient in this alloy to remove the retained austenite but not sufficient to subsequently coarsen the ferrite, previous work shows that coarsening occurs after the austenite has decomposed, and is associated with a large drop in hardness [21, 25, 26, 32].

These calculations support a correlation between the amount of hydrogen at saturation and the predicted grain boundary surface area per unit volume, rather than simply to the volume fraction of austenite (see table 3). As a result of the displacive

transformation to carbide—free bainite, the grain boundaries will be predominantly of a single orientation relationship. The austenite/bainitic ferrite interface is also associated with large dislocation densities in the austenite and ferrite, which are known to be trapping sites for hydrogen.

## 4 Discussion

Transformation to a nanostructure of bainitic ferrite and retained austenite has resulted in a large capacity for hydrogen trapping. The saturation levels of 7.1–8.5 ppmw can be expected to provide improved resistance to hydrogen embrittlement when low levels of hydrogen are introduced. In this saturated condition the elongation was greatly reduced, however the large trapping capacity may be advantageous in service conditions, and the presence of austenite can also be expected to lower the rate of hydrogen diffusion which may also further delay fracture. With regard to the trapping of hydrogen it should be noted that the strength of the trapping site and location may also be expected to be important. It may be that the introduction of strong trapping sites associated with carbides would be more beneficial in lowering diffusible hydrogen in the matrix.

Solano-Alvarez *et al.* have conducted thermal desorption experiments in 52100 steel, transformed to martensite with 12% retained austenite and carbides present. After saturation with hydrogen 7 ppmw was desorped by heating to 673 K, increasing to more than 9 ppmw after introducing micro-cracks by heat treatment, this suggests incoherent phases can be used to introduce strong trapping sites [32].

In the evolution curves observed the presence of austenite is associated with a shift in the desorption peak to around 498 K (225°C) from 383 K (110°C). At saturation, the diffusible hydrogen level was similar in the three conditions observed, with evolution

curve similar below 383 K (110°C). It is possible to introduce stronger trapping sites by the introduction of appropriate carbide particles [33], in this case the fine scale of the bainitic microstructure could be beneficial in further work by allowing a very fine dispersion of carbides due to precipitation at the plate boundaries [25, 26].

The three conditions of the steel examined suffered from low elongation after hydrogen embrittlement, reducing to 2–5% of the previous value. Steel A in the tempered condition has a lower calculated hydrogen embrittlement factor, but this is due to the lower initial elongation, rather than better absolute value.

There is a striking similarity of the fracture surfaces at high resolution when comparing the as heat-treated and the hydrogen charged material in each case, except that the material where hydrogen has been introduced has in addition a large amount of secondary cracking. Microplasticity of the brittle surface has previously been claimed to be evidence of the hydrogen enhanced plasticity mechanism [35]. However, cleavage in iron is well known to be associated with microscopic plasticity [36]. In these materials the microplasticity was evident irrespective of the presence of hydrogen and voids are present at the scale of 1 micrometer due to the high strength.

In TRIP-aided steels correlation has been observed between total hydrogen concentration after charging and the initial volume fraction of retained austenite [37]. Also, in TRIP-aided steels with bainitic ferrite matrix the addition of aluminium has been observed to increase the mechanical stability of austenite (with regards to hydrogen-assisted or stress-assisted transformation to martensite) by increasing its enrichment in carbon [37]. A similar effect has been observed in high-manganese austenitic steels, where the effect of aluminium on the stacking fault energy increases the

resistance to hydrogen embrittlement by reducing the tendency to form twin-boundary sites susceptible to embrittlement [22].

The high volume fraction of austenite can be expected to increase the resistance to hydrogen embrittlement by introducing trapping sites either in the austenite, or in the form of the large area of interface between the fine bainite plates and thin films of austenite.

Correlation of the total hydrogen content after saturation and the grain boundary surface area per unit volume indicates that this is the preferred location for trapping. This suggests that greater trapping should be observed in carbide-free bainitic steels with smaller bainite plate size, e.g. by transformation at lower temperature or change of alloy content, since a larger density of boundaries can be introduced.

It is possible that this trapping occurs in the austenite due to higher solubility limit; or at ferrite-austenite boundaries [41], perhaps a result of the lower diffusivity in austenite, or the greater disorder at the boundary. Previous work has demonstrated that trapped hydrogen is rendered innocuous [42] and others have developed strategies with the aim of reducing the amount of diffusible hydrogen, for example by engineering of carbides [33, 43, 44]. It is expected that austenite may contribute to the trapping, but the strength of the various trapping sites can also be expected to be of importance to the amount of diffusible hydrogen present.

Steels with a trapping capacity greater than 3 parts per million by weight (ppmw) are expected to have excellent resistance to hydrogen embrittlement [5, 45]. In this paper we have demonstrated that austenite content above 30 vol% results in trapping above 7 ppmw, and observed the large deterioration in properties that occurs when the steel is saturated in hydrogen. However, hydrogen susceptibility at levels expected from

environmental exposure has not been assessed. In service conditions, permeating retained austenite may be expected to aid resistance to hydrogen by lowering the diffusion rate of hydrogen through the microstructure, slowing absorption.

A concern has been that retained austenite may lead to uptake of hydrogen during processing, leading to embrittlement – specifically in the case of intercritical annealing and galvanizing of sheet steels as used in the automotive industry. DeCooman has highlighted the fact that hydrogen embrittlement of transformation induced plasticity (TRIP) aided steels has only been observed as a result of hydrogen charging experiments [38, 39], conditions unlikely to occur in automotive applications [40] and that the presence of hydrogen in the atmosphere during annealing does not necessarily result in increased hydrogen content of the steel, and hardly alters tensile properties in a range of TRIP-aided steels with yield strength 500-700 MPa and tensile strength 700–960 MPa [40].

## **5 Conclusions**

Despite the large quantity of austenite there was no demonstrated advantage conferred to the prevention of embrittlement after saturation with hydrogen.

After saturation with hydrogen fracture surfaces exhibited greater tendency towards quasi-cleavage although areas exhibiting plasticity were also observed.

As could be expected from the higher solubility of hydrogen in austenite, the presence of austenite in the structure was associated with greater hydrogen contents after charging. However, our analysis suggests a stronger correlation between the total hydrogen content and the total area of austenite–ferrite boundaries. A prediction based

on this observation is that transformation at lower temperatures should result in greater ability for trapping of hydrogen for the same austenite volume fraction.

## 6 Acknowledgements

It is gratifying to thank Prof A. L. Greer and Prof Sir H.K.D.H. Bhadeshia for provision of laboratory equipment and funds to carry out this work.

## References

- [1] J. P. Hirth. *Metall. Trans. A*, 11A:861, 1980.
- [2] I. M. Bernstein. In I. M. Bernstein and A. W. Thompson, editors, *Hydrogen Effects in Metals*, pages 3–11, 1996.
- [3] H.K.D.H. Bhadeshia. *Prog. Mater. Sci.*, 57:268–435, 2012.
- [4] H. Okada. Stress corrosion cracking and hydrogen cracking of structural steels. In *Proc. Int. Conf. SCC and HE of Iron base alloys. NACE-5*, pages 124–134. NACE.
- [5] T. Tarui and S Yamasaki. *Tetsu-to-Hagane/J. Iron Steel Inst. Japan*, 88:612–619, 2002.
- [6] S. Matsuyama. In *Delayed Fracture*. Nikkan Kogyo Shinbun Ltd, Tokyo, 1989.
- [7] T. Hojo, S. Song, K. Sugimoto, A. Nagasaka, S. Ikeda, H. Akamizu, and M. Mayuzumi. *Tetsu-to-Hagané*, 90:177–182, 2004.
- [8] F. G. Caballero, H.K.D.H. Bhadeshia, K. J. A. Mawella, D. G. Jones, and P. Brown. *Mater. Sci. Technol.*, 18:279–284, 2002.
- [9] C. Garcia-Mateo, F. G. Caballero, and H.K.D.H. Bhadeshia. *J. Phys.*, 112:17–25, 2003.
- [10] C. Garcia-Mateo, F. G. Caballero, and H.K.D.H. Bhadeshia. *ISIJ Int.*, 43(11):1821–1825, 2003.
- [11] C. Garcia-Mateo, F. G. Caballero, and H.K.D.H. Bhadeshia. *ISIJ Int.*, 43(8):1238–1243, 2003.
- [12] C. Garcia-Mateo, F. G. Caballero, and H.K.D.H. Bhadeshia. *Mater. Sci. Forum*, 500–501:495–502, 2005.
- [13] M. Peet, P. Hill, M. Rawson, S. Wood, and H.K.D.H. Bhadeshia. *Mater. Sci. Technol.*, 27(1):119–123, 2011.
- [14] H.K.D.H. Bhadeshia. *Mater. Sci. Technol.*, pages 1293–1302, 2005.

- [15] H. S. Hasan, M. Peet, H.K.D.H. Bhadeshia, S. Wood, and E. Booth. *Mater. Sci. Technol.*, 26:453–456, 2010.
- [16] M. J. Peet, S. S. Babu, M. K. Miller, and H.K.D.H. Bhadeshia. *Scr. Mater.*, 50:1277–1281, 2004.
- [17] S. S. Babu, E. D. Specht, S. A. David, E. Karapetrova, P. Zschack, M. Peet, and H.K.D.H. Bhadeshia. *Metall. Mater. Trans. A*, 36A:3281–3289, 2005.
- [18] H. J. Stone, M. J. Peet, H.K.D.H. Bhadeshia, P. J. Withers, S. S. Babu, and E. D. Specht. *Proc. R. Soc. London, Ser. A*, pages 1009–1027, 2008.
- [19] F. G. Caballero, M. K. Miller, A. J. Clarke, and C. Garcia-Mateo. *Scr. Mater.*, 63:442–445, 2010.
- [20] C.N. Hulme-Smith, M. J. Peet, I. Lonardelli, A. C. Dippel, and H.K.D.H. Bhadeshia. *Mater. Sci. and Technol.*, 31(2):254–256, 2015.
- [21] H. S. Hasan, M. J. Peet, M-N. Avettand-Fenoel, and H.K.D.H. Bhadeshia. *Mater. Sci. Eng. A*, 615:340–347, 2014.
- [22] J. H. Ryu, S. K. Kim, C. S. Lee, D.-W. Suh, and H.K.D.H. Bhadeshia. *Proc. R. Soc. A*, 469, 2013. 20120458.
- [23] X. Sun, J Xu, and Y Li. *Mater. Sci. Eng. A*, 114:179–187, 1989.
- [24] Lucy Fielding, Eun Ju Song, Do-Kyeong Han, Harshad Bhadeshia, and Dong-Woo Suh. *Proc. R. Soc. London A*, 470(2168):20140108, 2015.
- [25] C. Garcia-Mateo, M. J. Peet, F. G. Caballero, and H.K.D.H. Bhadeshia. *Mater. Sci. Technol.*, 20:814–818, 2004.
- [26] M. J. Peet. PhD thesis, University of Cambridge, 2010. Available online e.g. at <http://mathewpeet.org/>.
- [27] H.K.D.H. Bhadeshia, S. A. David, J. M. Vitek, and R. W. Reed. *Mater. Sci. Technol.*, 7(8):686–698, 1991.
- [28] W. Urushihara, F. Yuse, T. Nakayama, Y. Namimura, and N. Ibaraki. *Kobe Steel Eng. Rep.*, 52(3):57–61, 2002.
- [29] P. Yan, Ö. E. Güngör, P. Thibaux, and H.K.D.H. Bhadeshia. *Sci. Technol. Weld. Joining*, 15:137–141, 2010.

- [30] P. Yan, Ö. E. Güngör, P. Thibaux, and H.K.D.H. Bhadeshia. *Adv. Mater. Res.*, 89–91:651–656, 2010.
- [31] S. B. Singh and H.K.D.H. Bhadeshia. *Mater. Sci. Eng., A*, pages 72–79, 1998.
- [32] H. S. Hasan, M. J. Peet, and H.K.D.H. Bhadeshia. *International journal of materials research*. 103, pages 1319–1324, 2012.
- [33] W. Solano-Alvarez, E. J. Song, D. K. Han, D. W. Suh and H.K.D.H. Bhadeshia *Metall. Mater. Trans. A*, 46A:665–673, 2015.
- [34] S. Yamasaki and H.K.D.H. Bhadeshia. *Mater. Sci. Technol.*, 19:723–731, 2003.
- [35] C. D. Beacham. *Metall. Trans.*, 3:437–451, 1972.
- [36] J. F. Knott. *Fundamentals of Fracture Mechanics*. Butterworths, London, 1981.
- [37] T. Hojo, K. Sugimoto, Y. Mukai, and S. Ikeda. *ISIJ Int.*, 48(6):824–829, 2008.
- [38] M. De Meyer, K. De Wit, and B. C. De Cooman. *Steel Res. Int.*, 71(12):511–518, 2000.
- [39] T. B. Hildich, S-B. Lee, J. G. Speer, and D. K. Matlock. In *Proceedings of SAE 2003 world congress and exhibition*, Detroit, MI, USA, March 2003.
- [40] B. C. De Cooman. *Curr. Opin. Solid State Mater. Sci.*, 8:285–303, 2004.
- [41] J. L. Gu, K. D. Chang, H. S. Fang, and B. Z. Bai. *ISIJ Int.*, 42:1560–, 2002.
- [42] K. Takai and R. Watanuki. *ISIJ Int.*, 43(4):520–526, 2002.
- [43] T. Kushida, N. Kuratomi, T. Kudoh, H. Matumoto, T. Tsumura, and F. Nakasato. *Tetsu-to-Hagané*, 82:297–302, 1996.
- [44] M. Kubota, T. Tarui, S. Yamasaki, and T. Ochi. Technical Report 91, 2005.
- [45] S. Yamasaki, M. Kubota, and T. Tarui. *Nippon Steel Tech. Rep.*, 80:50–55, 1999.

Sample	Austenite			Ferrite
	Volume /%	LP /Å	C / wt%	LP /Å
A-563	35.1±0.1	3.61650±0.002	1.09±0.06	2.86412±0.0003
A-563-573	36.1±0.2	3.62006±0.001	1.20±0.02	2.86325±0.001
A-563-773	0	N/A	N/A	2.86911±0.002
B-563	30.0±0.1	3.63334±0.002	1.40±0.07	2.87297±0.002

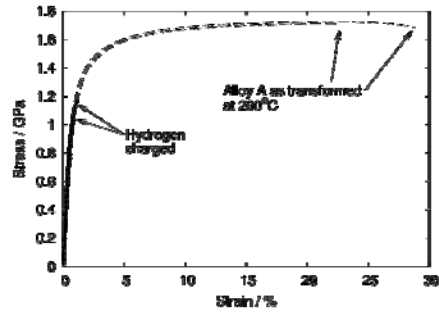
Table 1: X-ray diffraction results, samples identification in the form Alloy-T1-T2 where T1 and T2 are the temperatures of isothermal transformation and tempering both in Kelvin.

Alloy	<i>TS</i>	<i>YS</i>	<i>TEI</i>	<i>UEI</i>	<i>RA</i>	Hardness /HV50	<i>HES</i> /%		
	/MPa	/MPa	/%	/%	/%		( <i>RA</i> )	( <i>TEI</i> )	( <i>TS</i> )
A	1710	1090	21.4	20.0	24	512±6	60.8	98.4	35.1
	1729	891	28.0	25.0	40				
	+H	1178	889	0.4	0.4	14			
		1055	909	0.4	0.4	11			
AT	1686	1212	2.25	2.25	9.0	493±9	-31.1	94.8	29.2
	1617	1273	2.6	2.6	11				
	+H	1220	1220	0.2	0.2	13			
		1119	1119	0.05	0.05	12			
B	1715	1372	9.1	4.0	37	518±8	71.4	98.6	19.2
	1702	1350	5.3	1.7	44				
	+H	1300	1300	0.1	0.1	12			
		1460	1460	0.1	0.1	11			

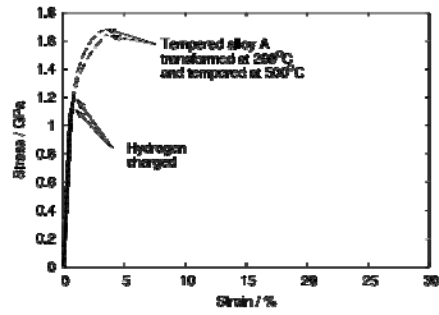
Table 2: Tensile test results, A - alloy A transformed at 563 K (290°C), AT - subsequently tempered at 773 K (500°C), B - alloy B transformed at 563 K (290°C), +H indicates hydrogen charged conditions. Tensile stress (*TS*), yield stress (*YS*), total elongation (*TEI*), uniform elongation (*UEI*), reduction in area (*RA*). Hydrogen embrittlement susceptibility (*HES*) for each property (*RA*, *TEI*, *TS*) expresses the hydrogen charged behavior in terms of initial property e.g. considering the reduction in area  $HES_{RA} = 100 \times (1 - RA_i / RA_0)$  where  $RA_i$  and  $RA_0$  are the instantaneous (charged) value and initial value respectively.

	Diffusible $H$ /ppmw	Total $H$ /ppmw	Total $H/VF_{\gamma}$ /ppmw	Total $H/VF_{\alpha}$ /ppmw
A	4.1	7.1	20.2	10.93
AT	1.8	3.0	N/A	3.0
B	5.2	8.5	28.3	12.14

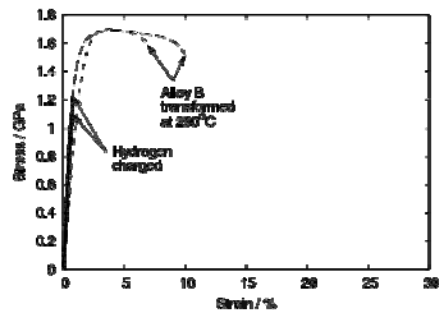
Table 3: Determination of hydrogen concentrations, alloys A and B transformed at 563 K (290°C), AT indicates alloy A tempered at 773 K (500°C).



(a) Alloy A

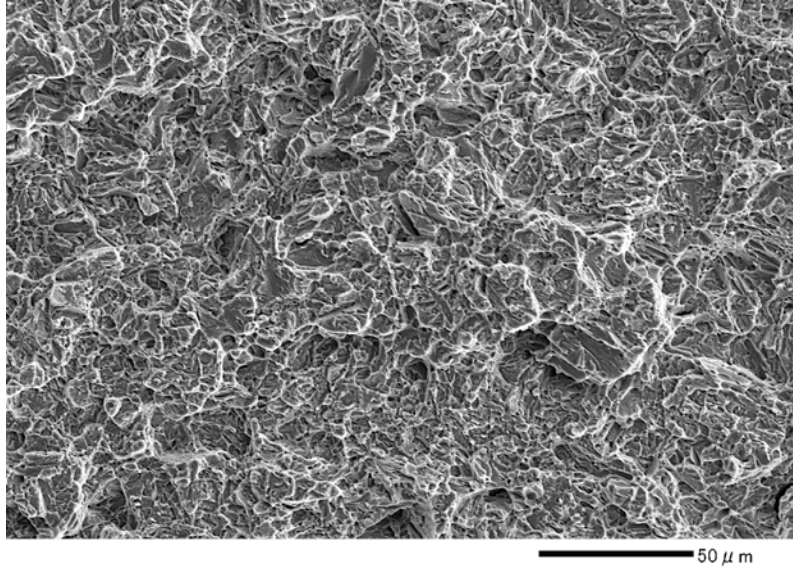


(b) Tempered A

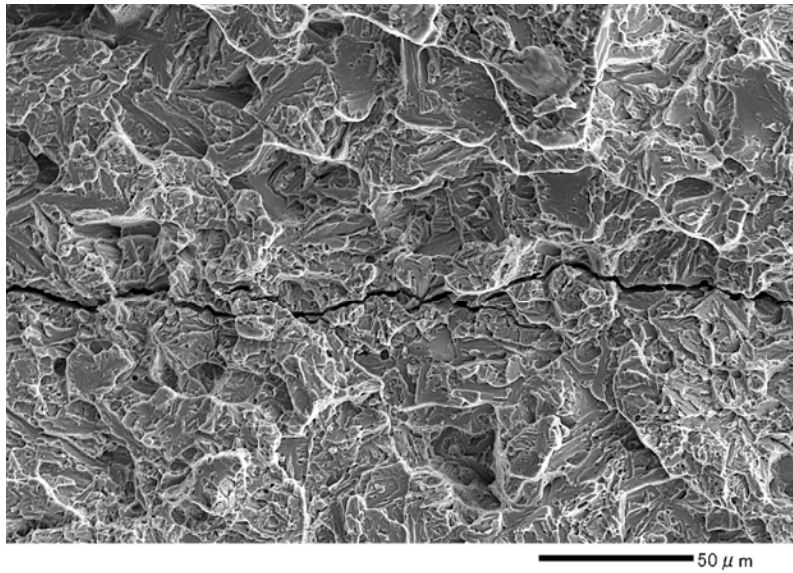


(c) Alloy B

Figure 1: Results of tensile testing, showing reduction of elongation by hydrogen charging.

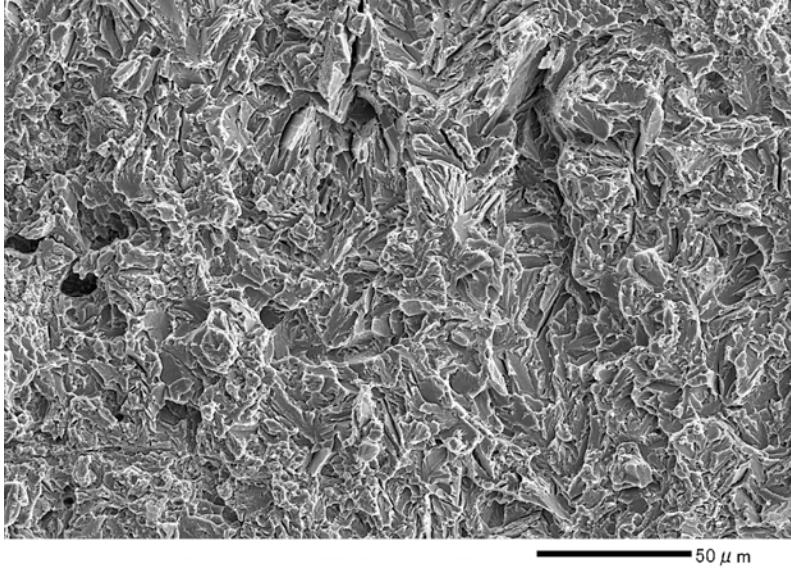


(a) As-transformed

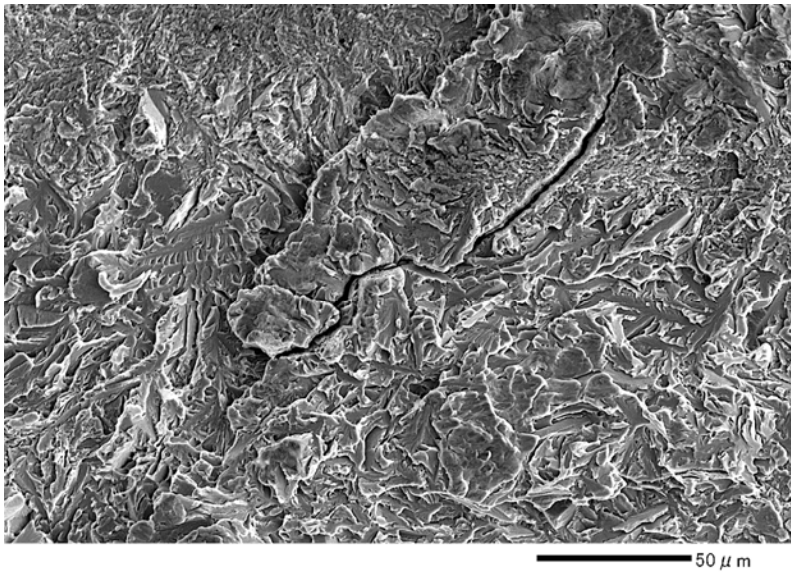


(b) After hydrogen charging

Figure 2: Steel A transformed at 563 K (290°C), effect of hydrogen charging on tensile fracture.

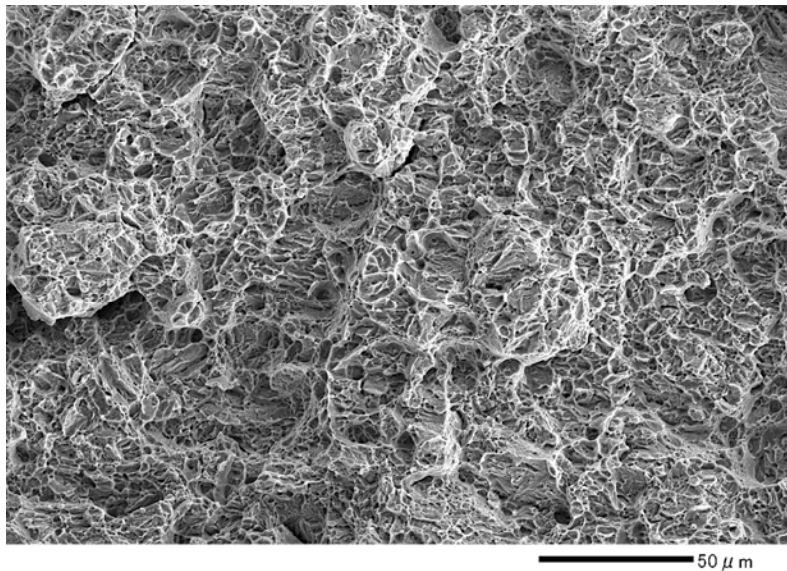


(a) As tempered

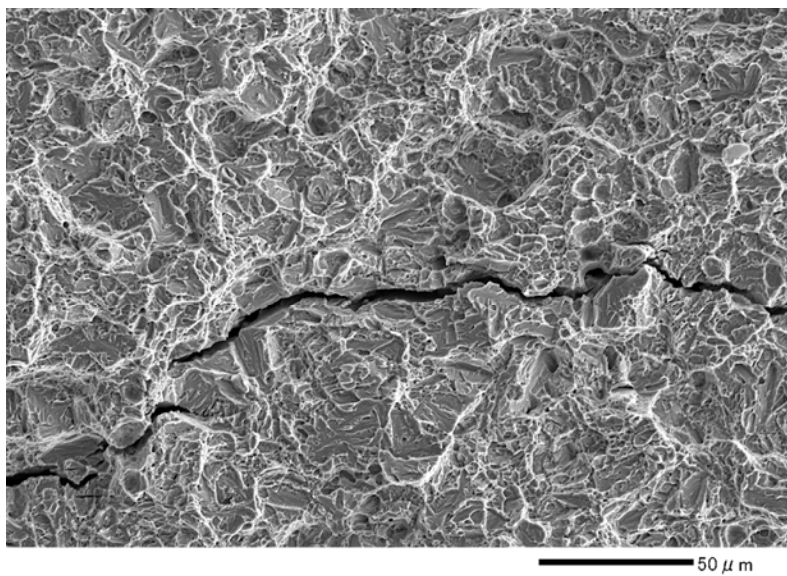


(b) After hydrogen charging

Figure 3: Steel A in tempered condition, transformed at 563 K (290°C) and tempered at 773 K (500°C), tensile fracture surfaces.

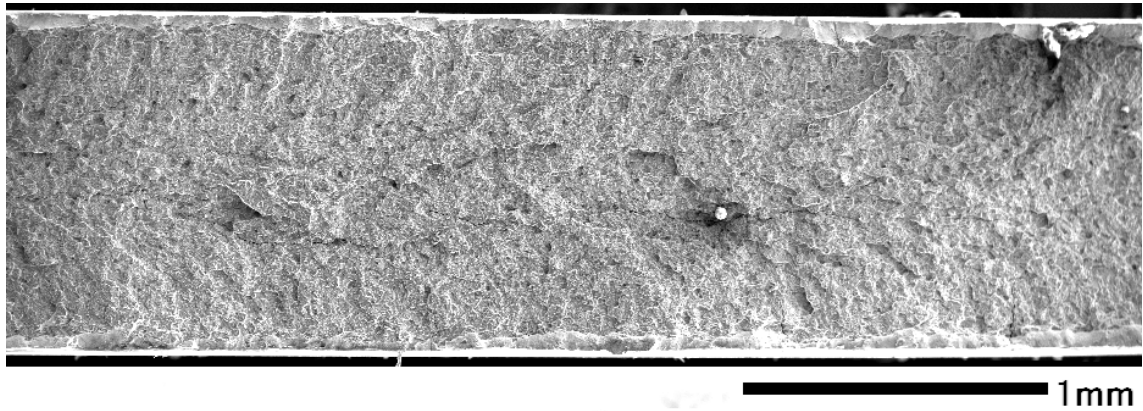


(a) As-transformed

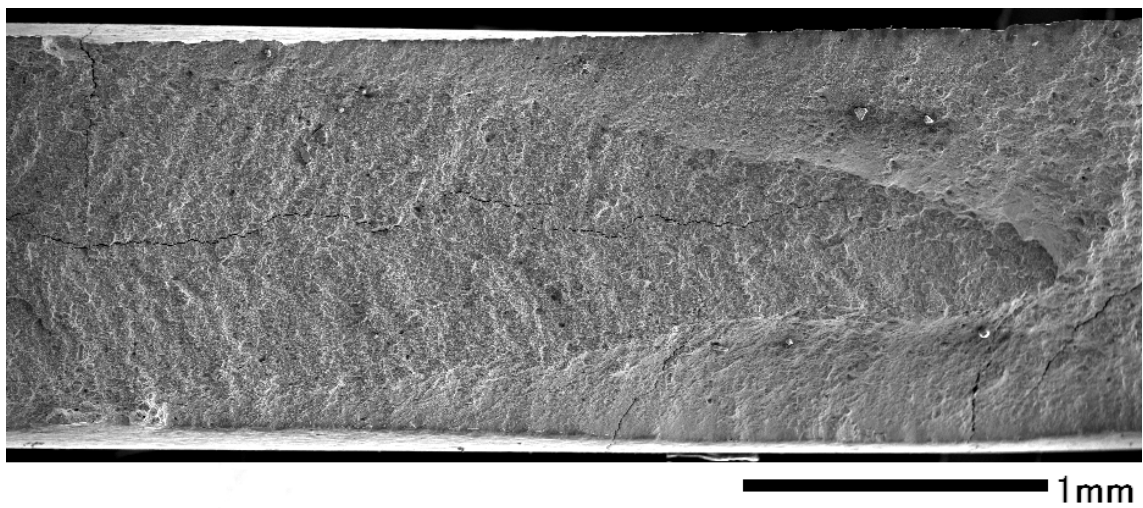


(b) After hydrogen charging

Figure 4: Steel B transformed at 563 K (290°C), effect of hydrogen charging on fracture.



(a) Steel A



(b) Steel B

Figure 5: Fracture surfaces of hydrogen charged samples at lower resolution, showing proportion of fracture surface which sheared. Images show approximately half the fracture surface with outer edge close to the image right hand side. Steel B exhibited greater amount of shearing both samples exhibit cracking after hydrogen charging.

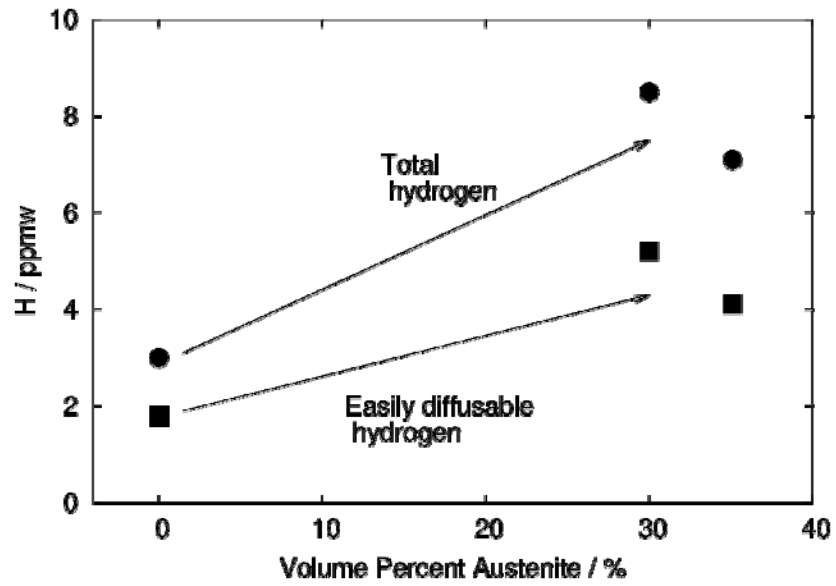


Figure 6: Results of hydrogen analysis, the total hydrogen and the diffusible hydrogen is greater in material with a large volume fraction of retained austenite.

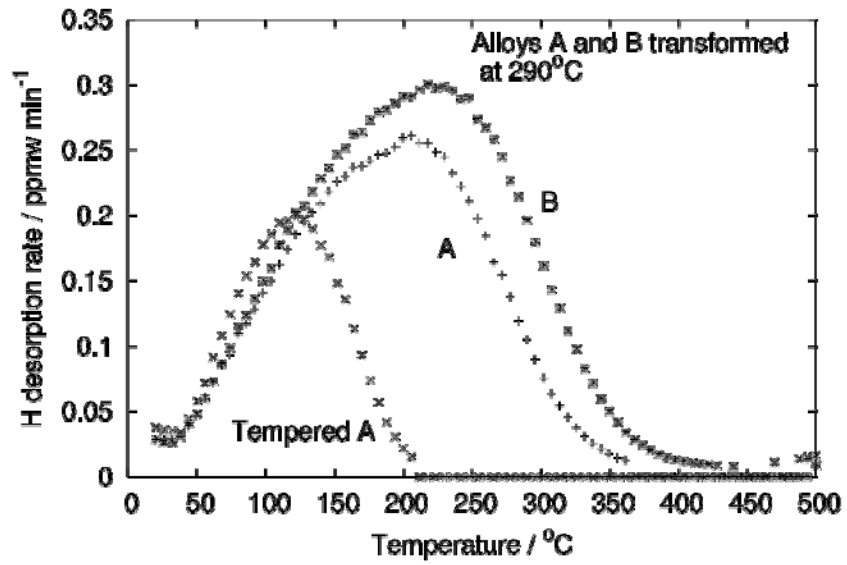
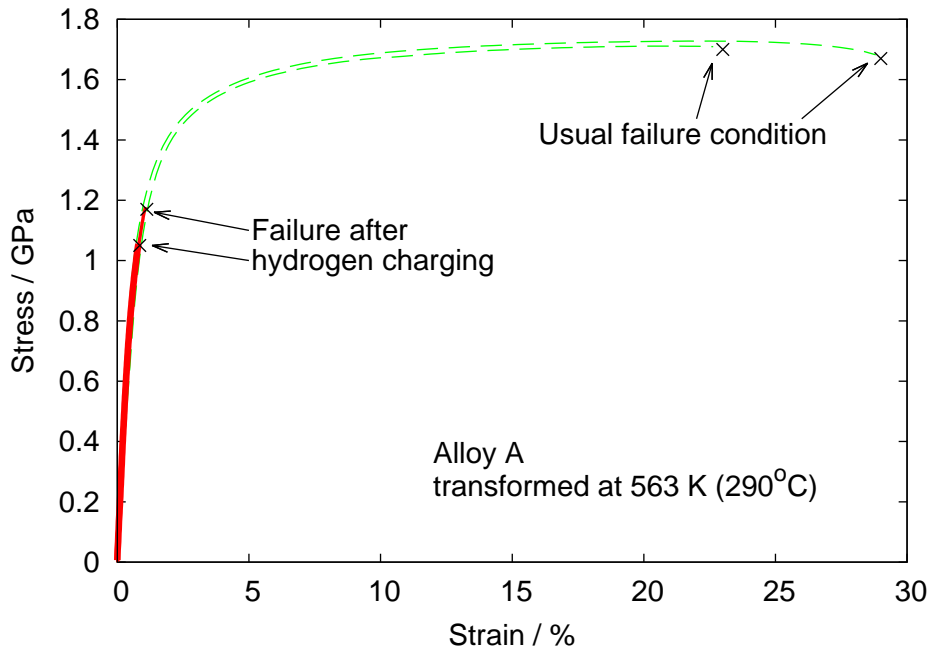
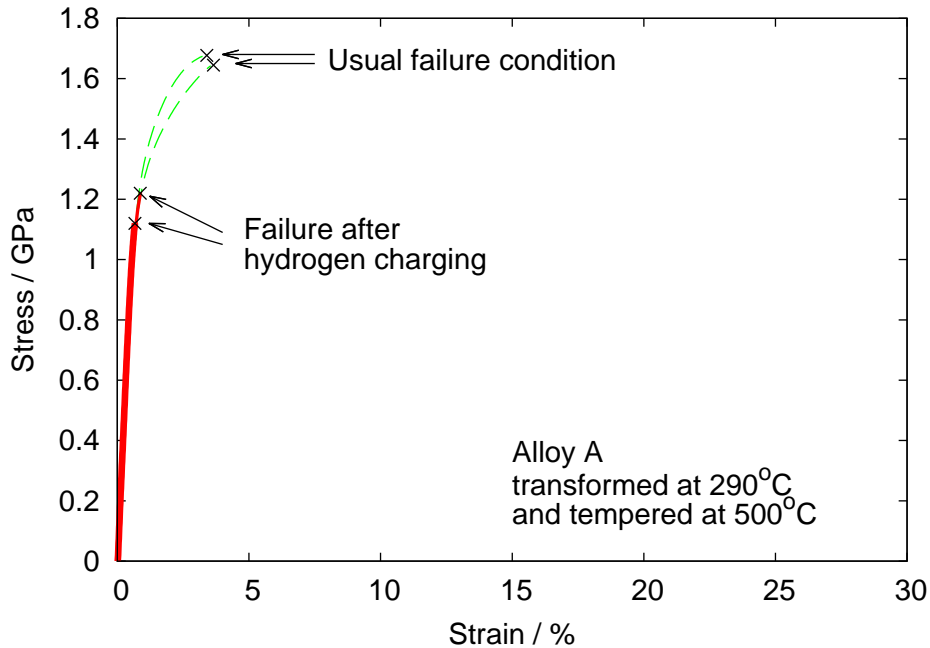
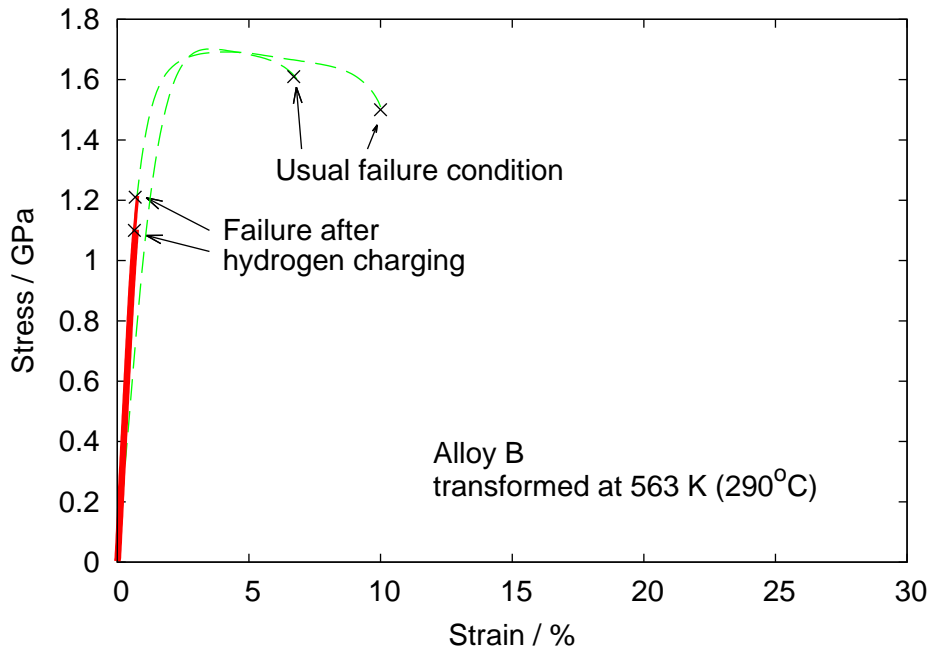
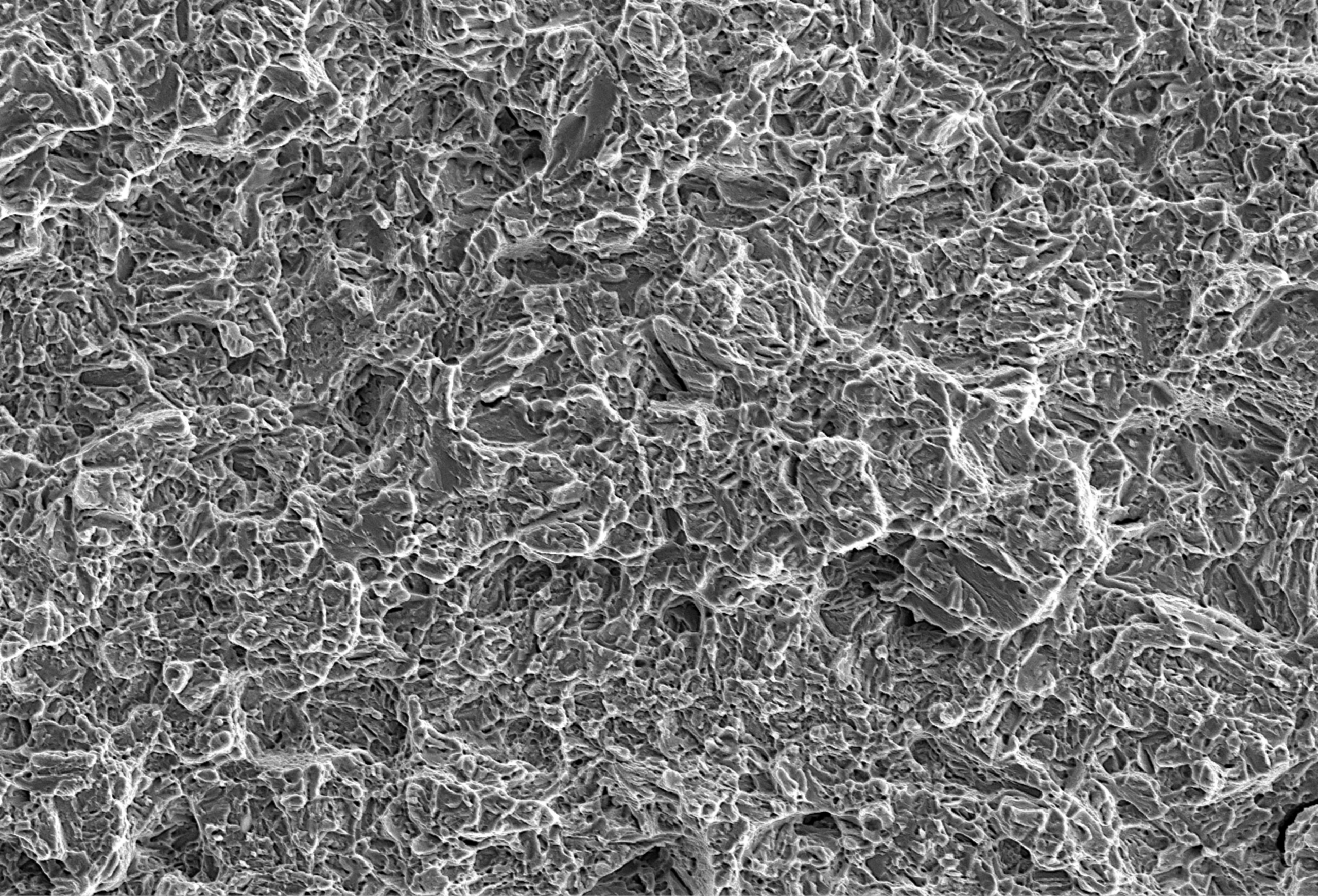


Figure 7: Comparison of evolution of hydrogen during heating for the relevant alloys and heat treatments.

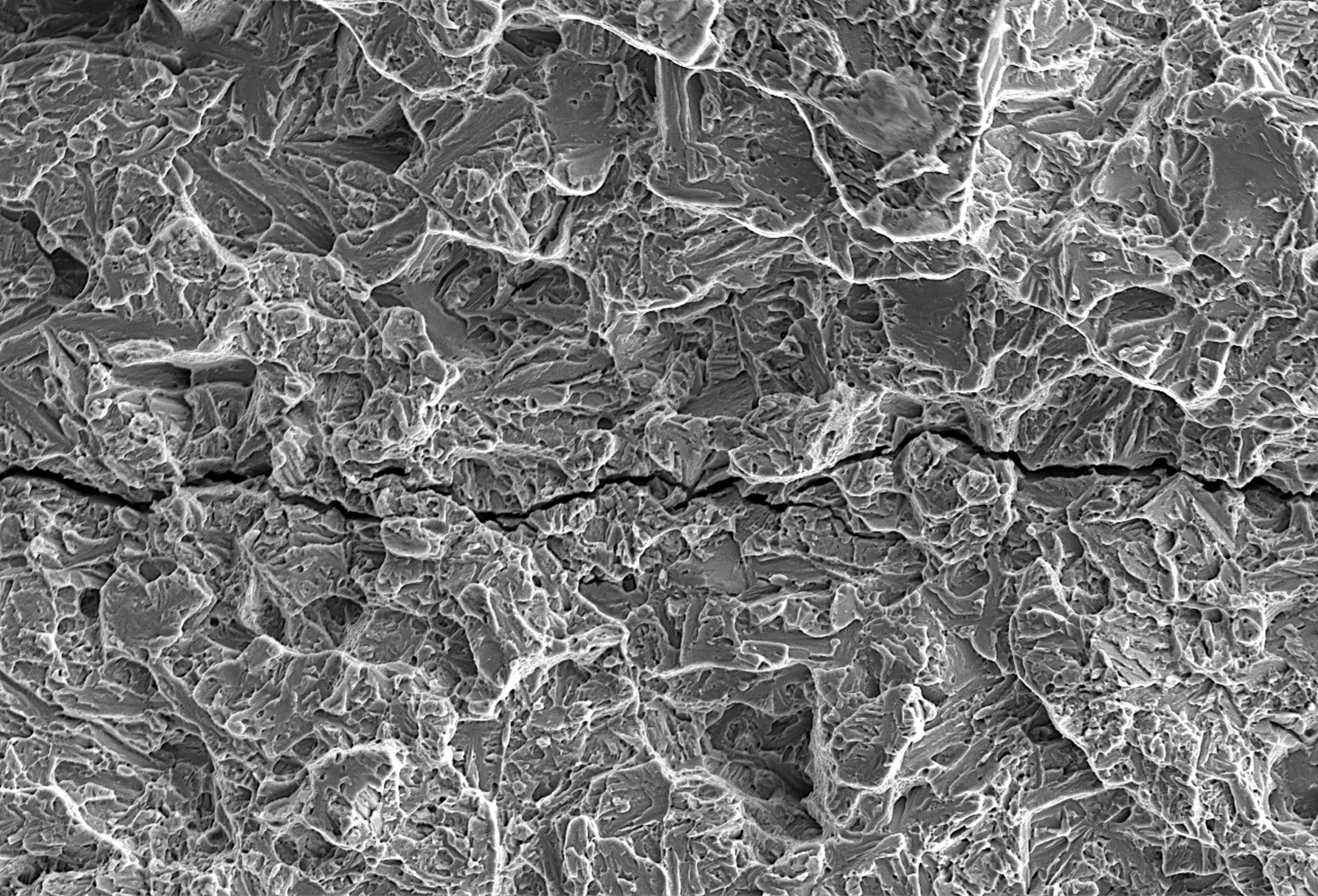




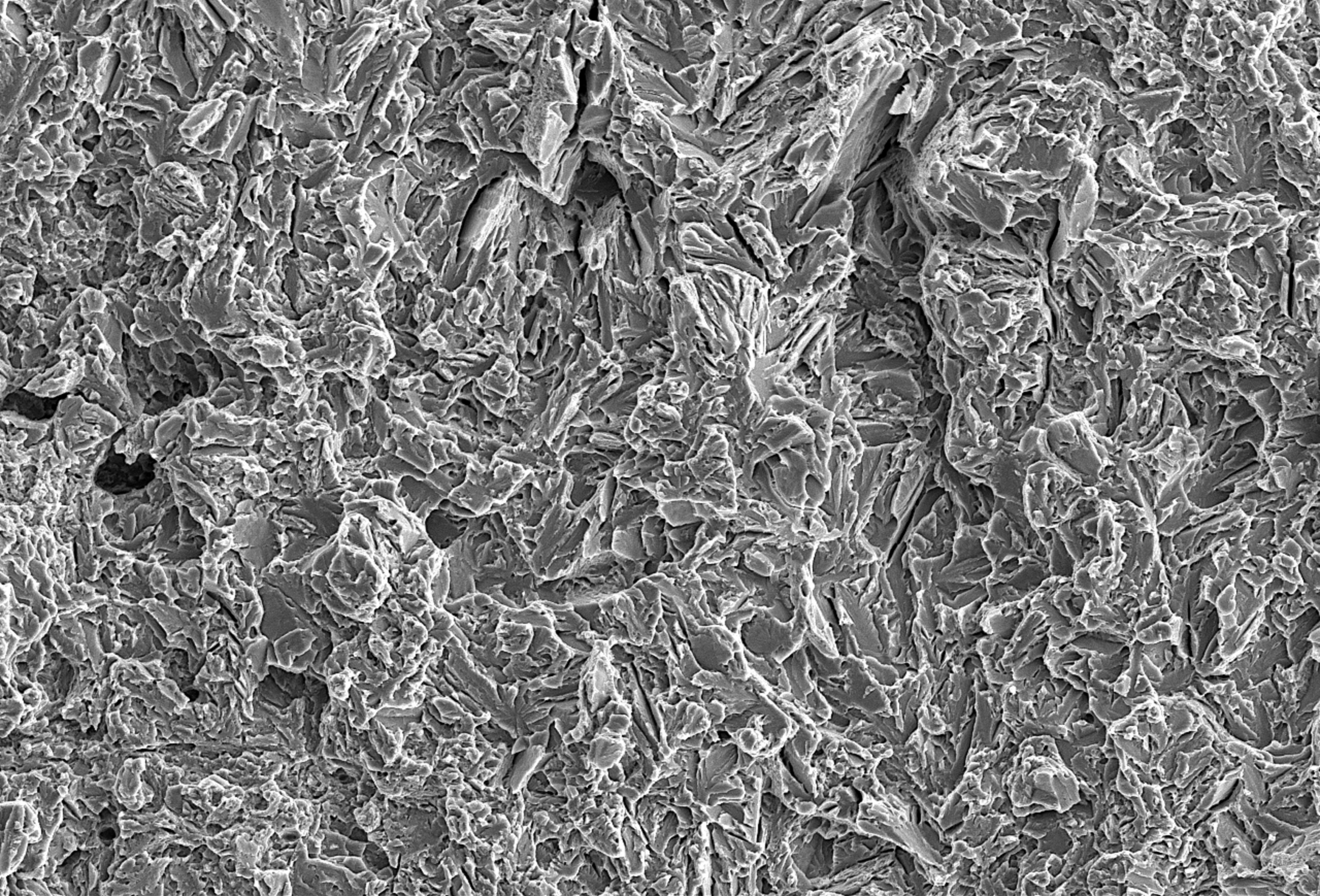




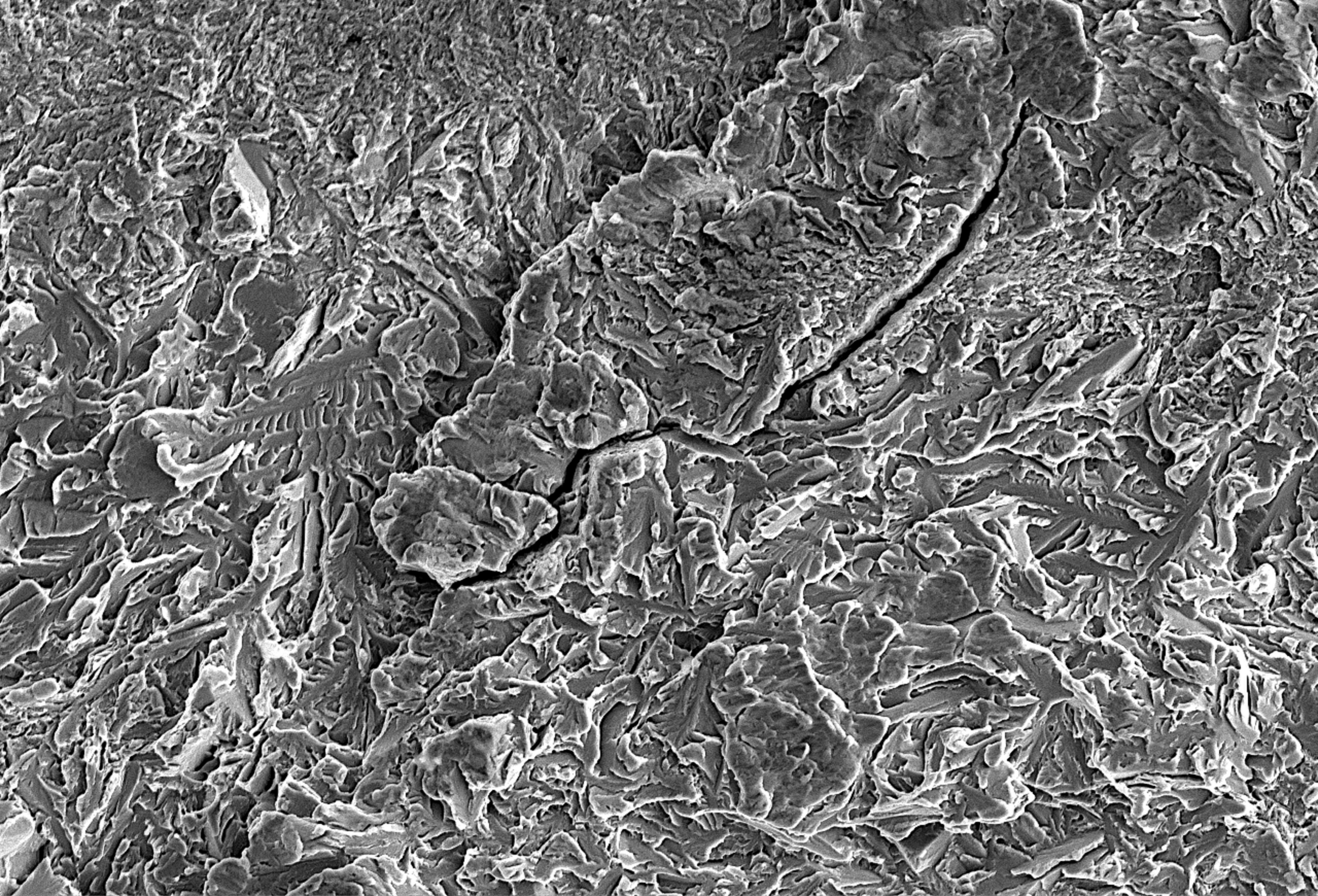
50  $\mu$  m



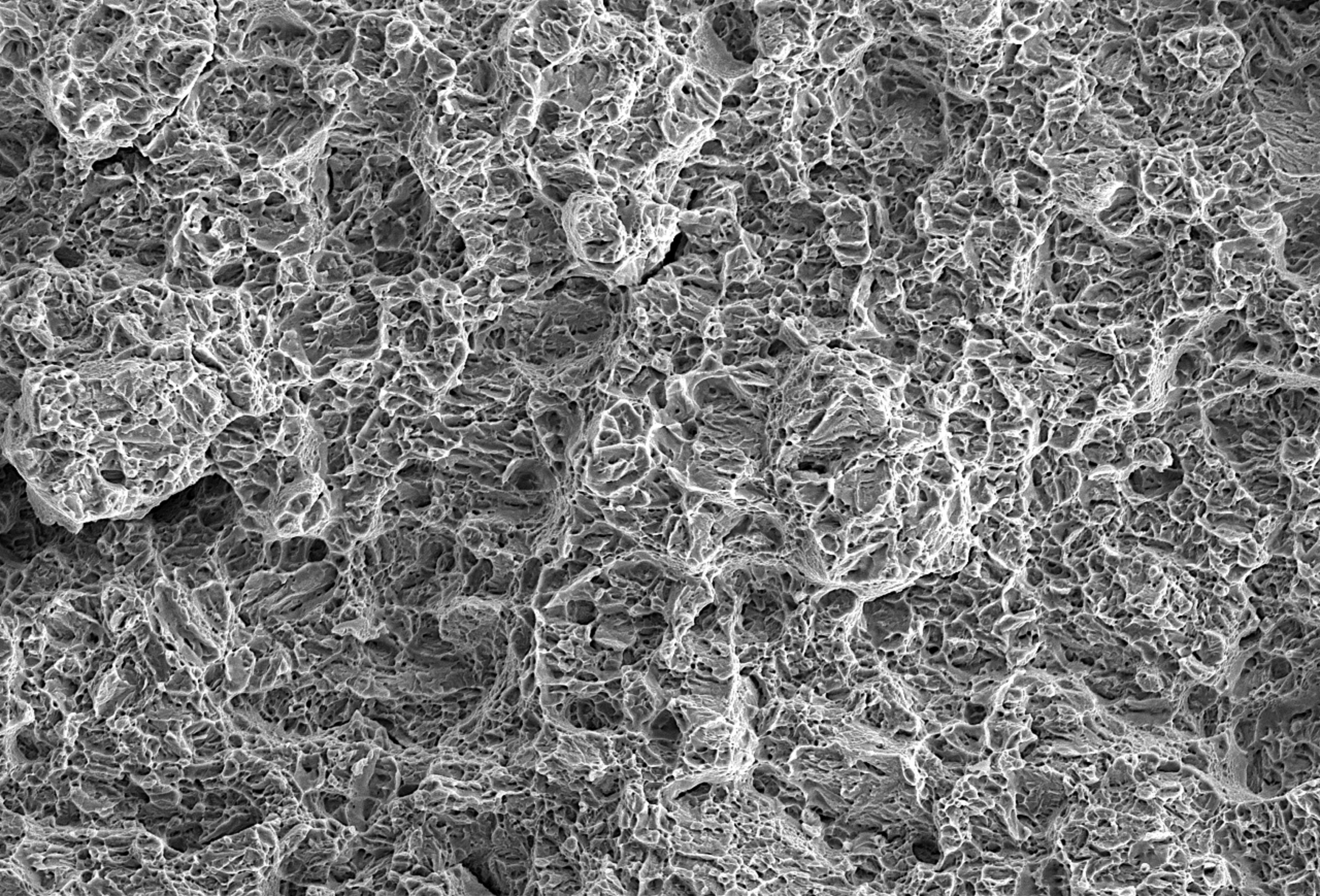
50  $\mu$  m



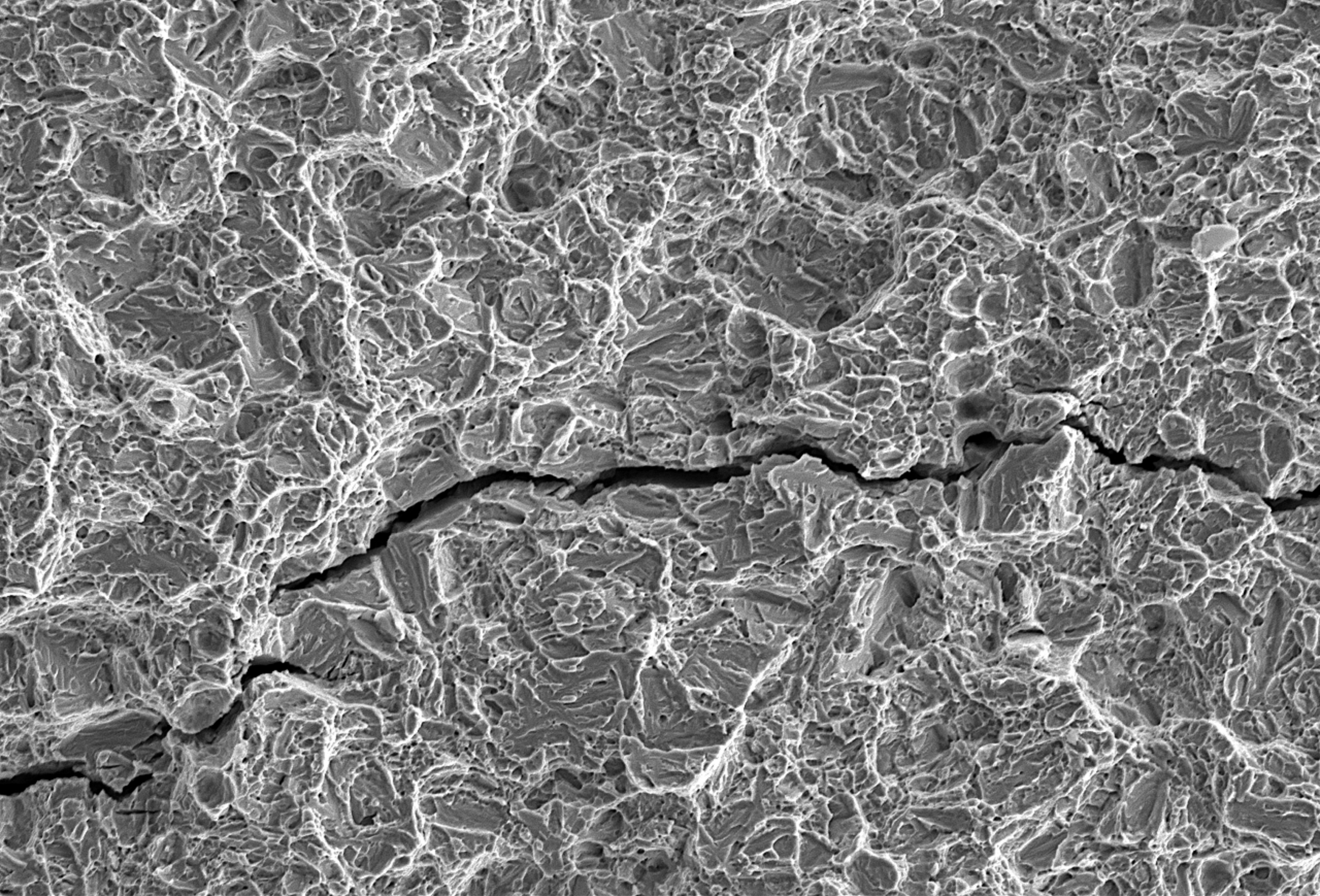
50  $\mu$  m



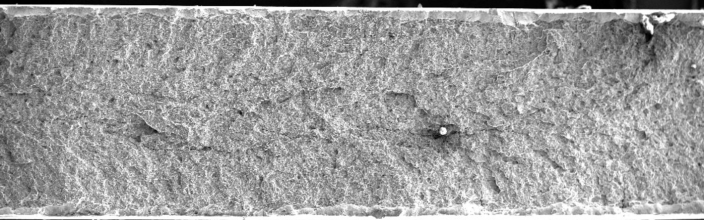
50  $\mu$  m



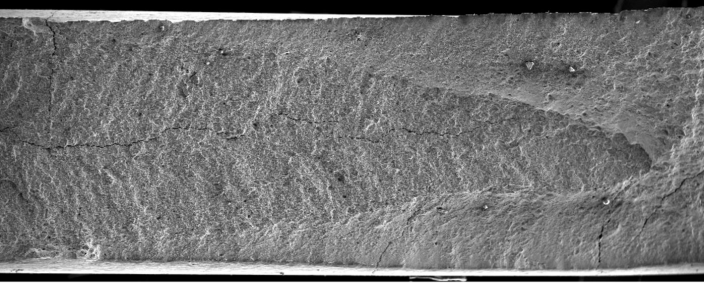
50  $\mu$  m



50  $\mu$  m



1mm



1mm

